

Either IL-7 activation of JAK-STAT or BEZ inhibition of PI3K-AKT-mTOR pathways dominates the single-cell phosphosignature of *ex vivo* treated pediatric T-cell acute lymphoblastic leukemia cells

Daniela Kuzilková,^{1,2*} Cristina Bugarin,^{3*} Katerina Rejlova,^{1,2} Axel R. Schulz,⁴ Henrik E. Mei,⁴ Maddalena Paganin,⁵ Alessandra Biffi,⁵ Andrea Biondi,³ Tomas Kalina^{1,2#} and Giuseppe Gaipa^{3#}

¹Childhood Leukemia Investigation Prague, Prague, Czech Republic; ²Department of Pediatric Hematology and Oncology, 2nd Faculty of Medicine, Charles University Prague, Prague, Czech Republic; ³Fondazione Tettamanti, Clinica Pediatrica Università degli Studi Milano Bicocca, Monza (MB), Italy; ⁴German Rheumatism Research Center Berlin (DRFZ), a Leibniz Institute, Berlin, Germany and ⁵Pediatric Hematology, Oncology and Stem Cell Transplant Division, Women and Child Health Department, University of Padova, Padova, Italy.

*DK and CB contributed equally as co-first authors.

#TK and GG contributed equally as co-senior authors.

Correspondence:

Andrea Biondi
andrea.biondi@unimib.it

Received: March 17, 2021


Accepted: October 12, 2021

Prepublished: October 21, 2021

<https://doi.org/10.3324/haematol.2021.278796>

©2022 Ferrata Storti Foundation

Haematologica material is published under a

CC BY-NC license 

Supplementary Tables

Table S1. Mass cytometry panel

Target	Metal	Clone	Function	Detection prior or after methanol permeabilization	Vendor	Catalogue number	Conjugation protocol
CD45	89Y	Hi30	barcoding	prior	Fluidigm	3089003B	vendor
CD45	104Pd	Hi30	barcoding	prior	Exbio	11-222-M001	
CD45	106Pd	Hi30	barcoding	prior	Exbio	11-222-M001	
CD45	108Pd	Hi30	barcoding	prior	Exbio	11-222-M001	
CD45	110Pd	Hi30	barcoding	prior	Exbio	11-222-M001	
HLA-I	113In	W6/32	immunophenotype	prior	Exbio	11-422-C100	
CD45	115In	MEM-28	barcoding	prior	Exbio	11-222-M001	
CD19	142Nd	HIB19	immunophenotype	prior	Fluidigm	3142001B	vendor
CD5	143Nd	UCHT2	immunophenotype	prior	Fluidigm	3143007B	vendor
CD4	145Nd	MEM-241	immunophenotype	prior	Exbio	11-359-C100	X8 labeling kit
CD8a	146Nd	RPA-T8	immunophenotype	prior	Fluidigm	3146001B	vendor
CD7	147Sm	CD7-6B7	immunophenotype	prior	Fluidigm	3147006B	vendor
CD34	148Nd	581	immunophenotype	prior	Fluidigm	3148001B	vendor
p-4E-BP1 [T37/T46]	149Sm	236B4	phospho-protein	after	Fluidigm	3149005A	vendor
p-STAT5 [Y694]	150Nd	47	phospho-protein	after	Fluidigm	3150005A	vendor
CD2	151Eu	TS1/8	immunophenotype	prior	Fluidigm	3151003B	vendor
p-AKT [S473]	152Sm	D9E	phospho-protein	after	Fluidigm	3152005A	vendor
BCL-2	153Eu	Bcl-2/100	apoptosis	after	Exbio	11-668-C100	X8 labeling kit
CD56	155Gd	B159	immunophenotype	prior	Fluidigm	3155008B	vendor
p-p38 [T180/Y182]	156Gd	D3F9	phospho-protein	after	Fluidigm	3156002A	vendor
TSLP-R	158Gd	1B4	immunophenotype	prior	Fluidigm	3158026B	vendor
p-S6 [S240/244]	159Tb	D68F8	phospho-protein	after	CST	5364	X8 labeling kit
CD38	160Gd	HIT2	immunophenotype	prior	Exbio	11-366-C100	X8 labeling kit

CD3	161Dy	UCHT1	immunophenotype	prior	Exbio	11-514-C100	X8 labeling kit
p-LCK [T505]	162Dy	4/LCK-	phospho-protein	after	Fluidigm	3162004A	vendor
TDT	164Dy	E17-1519	immunophenotype	after	Fluidigm	3164015B	vendor
p-CREB [S133]	165Ho	87G3	phospho-protein	after	Fluidigm	3165009A	vendor
p-RB [S807/811]	166Er	J112-906	proliferation	after	Fluidigm	3166011A	vendor
Ki-67	168Er	B56	proliferation	after	Fluidigm	3168007B	vendor
CD33	169Tm	WM53	immunophenotype	prior	Fluidigm	3169010B	vendor
Cl.Caspase3 (D175)	170Er	poly	apoptosis	after	CST	9661	X8 labeling kit
p-ERK1/2	171Yb	D13.14.4E	phospho-protein	after	Fluidigm	3171010A	vendor
PTEN	172Yb	A2B1	tumor supressor	after	BD	559600	X8 labeling kit
HLA-DR	174Yb	L243	immunophenotype	prior	Fluidigm	3174001B	vendor
MYC	176Yb	9E10	trancriptionfactor	after	Fluidigm	3176012B	vendor
DNA	191Ir		DNA intercalator	after	Fluidigm	201192B/201192A	vendor
CD45	194Pt	MEM-28	barcoding	prior	Exbio	11-222-M001	²
HLA-I	198Pt	W6/32	barcoding	prior	Bxcell	BE0079	²

CST, Cell Signaling Technology; BD, BD Biosciences; metOH, methanol

Table S2. Early response to therapy and signaling *in vitro* response to IL-7 or BEZ-235 in 16 studied T-ALL patients

code	PDN response	% MRD at day 15 by flow cytometry *	Signaling response to IL7	Signaling response to BEZ-235	Relapse** (Yes/Not)/site	Time of relapse [§]	Status (Alive/Dead)
TALL-1	PGR	nd	yes	no	Y/BM	early	D
TALL-2	PPR	30.0%	no	no	Y/BM	very early	D
TALL-3	PGR	nd	yes	no	N	-	A
TALL-4	PGR	nd	yes	no	Y/SNC	early	A
TALL-5	PGR	2.0%	yes	yes	N	-	A
TALL-6	PPR	70.0%	no	yes	N	-	A
TALL-8	PGR	1.15%	no	yes	N	-	nd
TALL-9	PGR	0.01%	no	yes	N	-	A
TALL-10	PPR	24.5%	no	yes	N	-	A
TALL-11	PGR	0.14%	yes	no	N	-	A
TALL-12	PPR	23.1%	no	yes	Y/BM	early	D
TALL-13	PGR	0.14%	yes	yes	N	-	A
TALL-14	PPR	61.9%	no	yes	N	-	A
TALL-15	PGR	1.30%	no	yes	Y/BM + kidney	early	A
TALL-16	PPR	90.1%	no	yes	Y/BM	late	A
TALL-17	PPR	0.99%	no	yes	Y/BM +SNC	early	D

*According to the criteria by Basso G et al. JCO 2009 the % of flow cytometry MRD in the BM of day15 identifies three patient's risk groups: standard (SR, 0.1% blasts), intermediate (IR, 0.1 to 10%) , and high (HR, ≥ 10); nd, not determined; CNS, Central Nervous System; ** relapse was defined by morphology and immunophenotype by of blasts %. § very early, < 18 months after primary diagnosis; early, ≥ 18 months after primary diagnosis and <6 months after completion of primary therapy; late, ≥ 6 months after completion of primary therapy (from IntReALL HR 2010 Protocol)

Table S3. The somatic mutation analysis of NOTCH1 gene according to the specific exons analyzed

Patient's code	NOTCH1 EXONS				
	exon 26	exon 27	exon 28	exon 34 TAD	exon 34 PEST
TALL-1	nd	nd	nd	nd	nd
TALL-2	wt	wt	wt	wt	wt
TALL-3	wt	wt	p.A1741_INS/DEL	wt	wt
TALL-4	p.L1585Q	wt	wt	wt	p.S2513F
TALL-5	wt	wt	wt	wt	wt
TALL-6	wt	wt	wt	wt	wt
TALL-8	wt	p.I1718T	wt	wt	wt
TALL-9	p.F1592_L1593ins	wt	wt	wt	wt
TALL-10	wt	wt	wt	wt	wt
TALL-11	p.L1585P	wt	wt	not detemined	wt
TALL-12	wt	wt	wt	wt	wt
TALL-13	p.H1591_F1592>XX	wt	wt	wt	wt
TALL-14	wt	wt	wt	wt	wt
TALL-15	not detemined	p.L1678P	wt	wt	not detemined
TALL-16	wt	wt	wt	wt	wt
TALL-17	wt	wt	wt	wt	wt

Supplementary Figure Legends

Figure S1: Phenotyping of T-ALL cells and T-cells with bivariate gating

T-ALL cell population was separated from residual nonmalignant T-cells using traditional bivariate gating. Residual T-cells are defined as CD45^{high}, CD7⁺, CD4 or CD8 single positive. T-ALL cells were defined as CD45^{dim}, CD7⁺, and homogenous major population on CD4 vs CD8 scatterplot. Additionally, both populations were gated for Cleaved Caspase 3 negativity

Figure S1

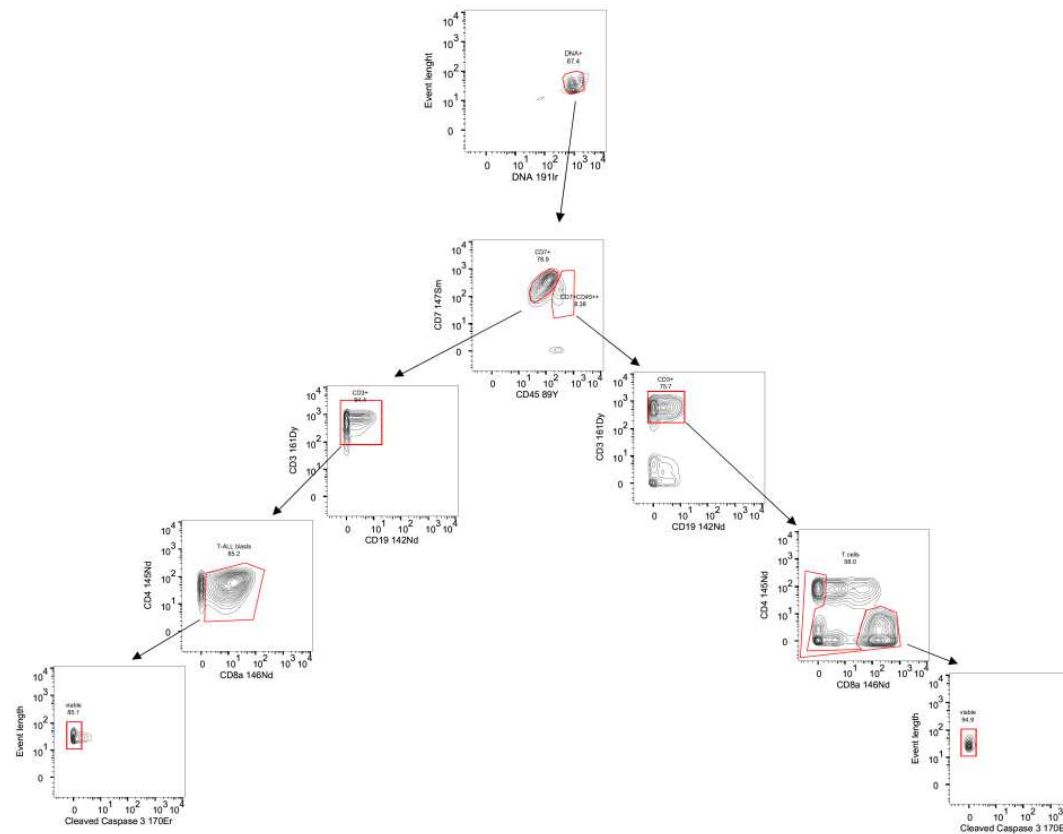


Figure S2: *Vaevictis* dimensionality reduction identifies dominant clone of T-ALL cells

Deep learning based *Vaevictis* dimensionality reduction (dim red) was applied on T-ALL cells obtained from 16 pediatric T-ALL patients at diagnosis. Signaling, proliferation and internal regulators (PTEN, MYC, BCL-2, p-4E-BP1, p-STAT5, p-AKT, p-p38, p-S6, p-LCK, p-CREB, p-RB, Ki-67, p-ERK1/2) were considered for the projection calculation. T-ALL cells from *PTEN* exon 7 mutated (*PTEN*mut) samples (n=6, orange label), T-ALL cells from samples harboring *NUP214/ABL1* gene fusion (n=2, red label) and T-ALL cells from *PTEN* wild type (*PTEN*wt) and *NUP214/ABL1* negative T-ALL samples (n=8, green label) are depicted. The gates represent dominant clone of T-ALL cells.

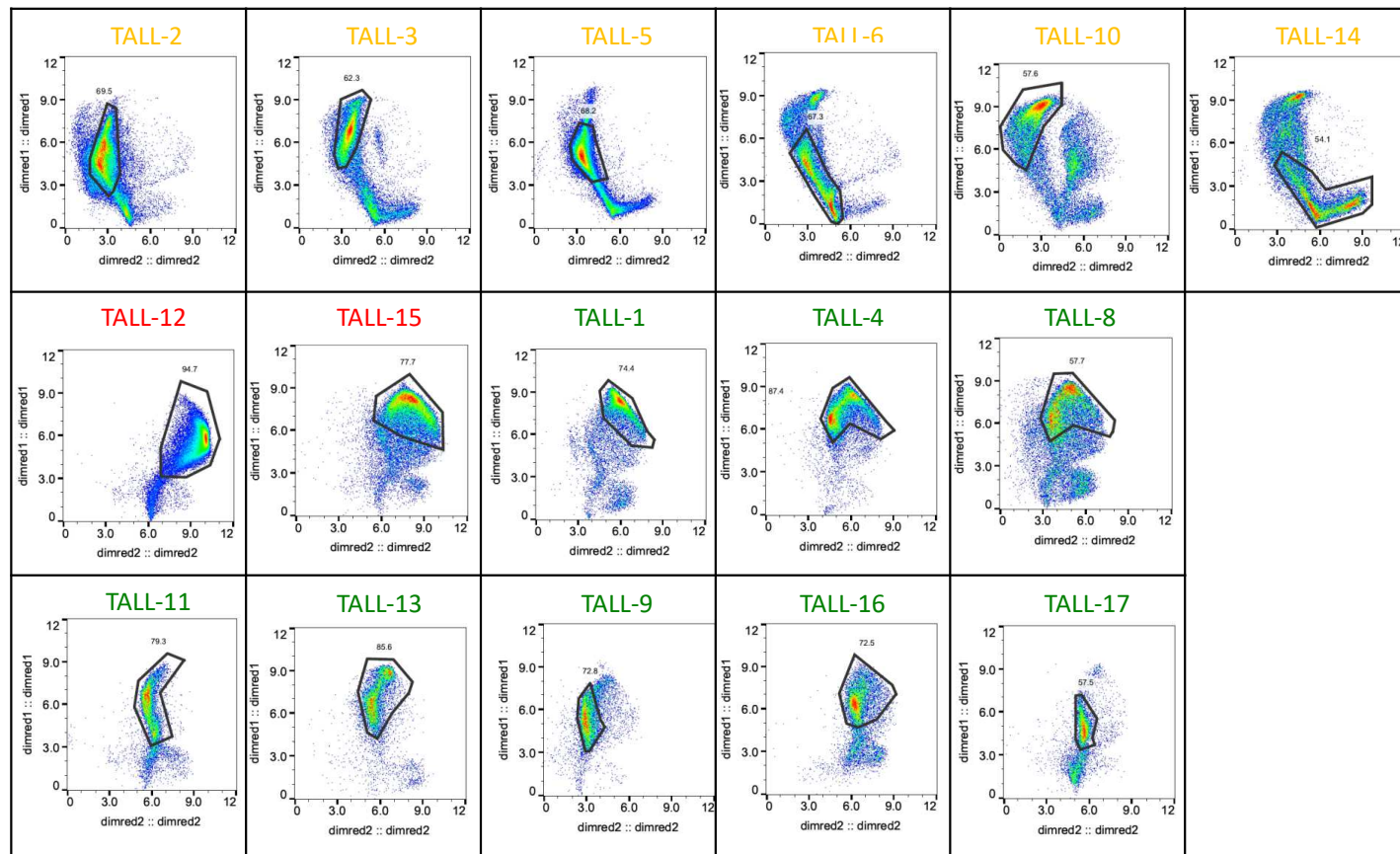
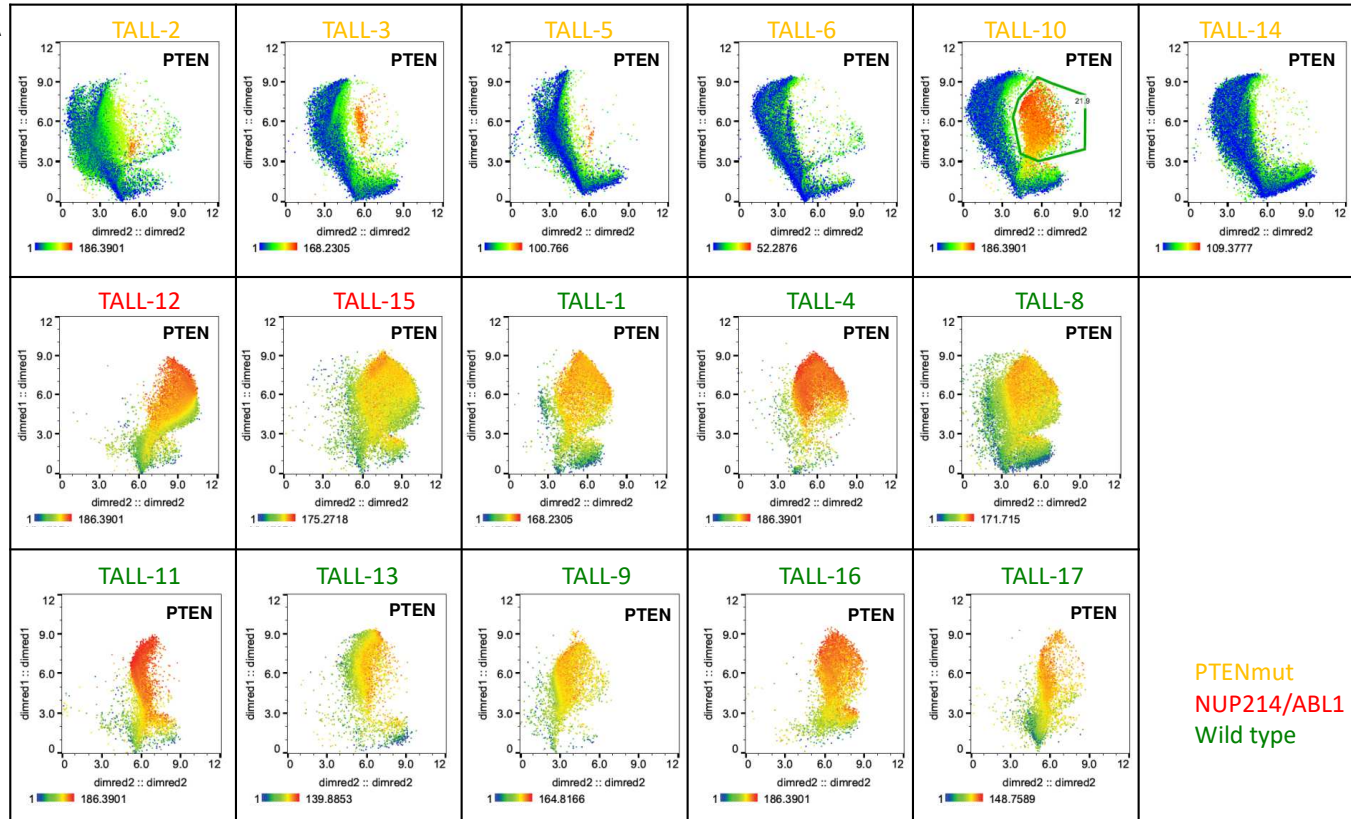


Figure S3: Vaevictis dimensionality reduction reveals the impact of PTEN and MYC expression on phospho-signature patterns in pediatric T-ALL cells

T-ALL cells from *PTEN*mut T-ALL samples (n=6, orange label), T-ALL cells from T-ALL samples harboring *NUP214/ABL1* gene fusion (n=2, red label) and T-ALL cells from T-ALL patients with *PTEN*wt and *NUP214/ABL1* negative T-ALL patients (n=8, green label) are depicted. Signaling, proliferation and internal regulators (n=13) were considered for the projection calculation. **(A)** The heat corresponds with expression of PTEN, note the scale max differ for each sample. **(B)** The heat corresponds with expression of MYC, note the scale max differ for each sample.

S3A



S3B

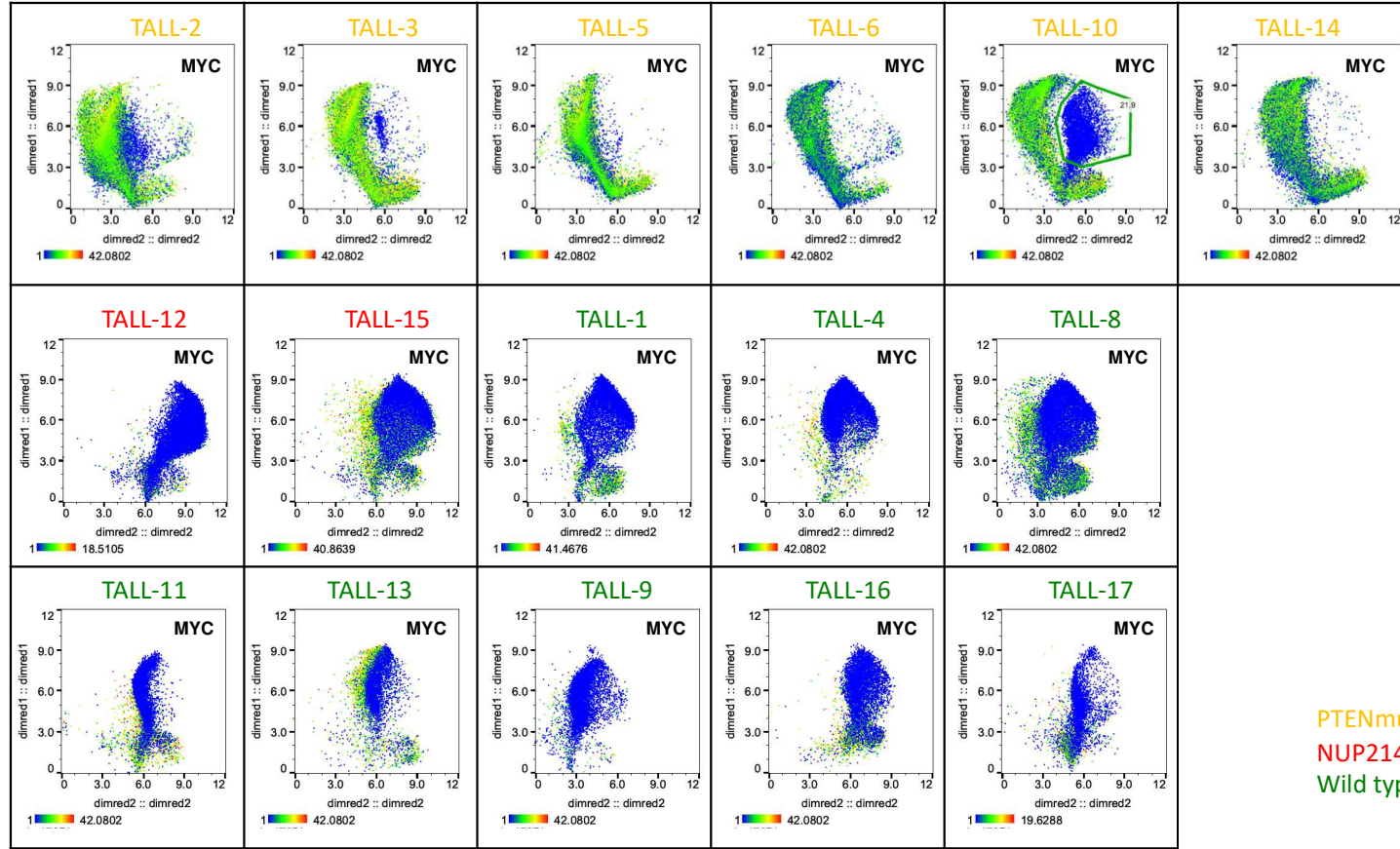


Figure S4: Residual T-cells show lower level of signaling activity and interpatient heterogeneity compared to T-ALL cells

Heatmap displays the arcsinh transformed median intensity of intracellular regulators in T-ALL cells (label in color) and residual T-cells (black label). Each row of squares shows the expression or phosphorylation of particular protein, while each column represents particular specimen. Hierarchical clustering with Euclidean distance metrics and an average linkage was used to dissect clusters (separated with horizontal lines) to find similarities between samples. Heat of each square corresponds with the level of expression/phosphorylation of indicated marker. Three distinct clusters can be resolved: (i) cluster of T-ALL cells with highly active signaling and proliferation markers, (ii) cluster of T-ALL cells with intermediate active signaling and proliferation markers and (iii) cluster of residual T-cells. Cluster with highly active signaling and proliferation markers includes the two patients with *NUP214/ABL1* gene fusion. Within cluster with intermediate activation level a separate cluster of T-ALL patients with *PTEN*mut is formed. One T-ALL patient sample showed low level of activation and it was assigned in the cluster enriched of residual T-cells

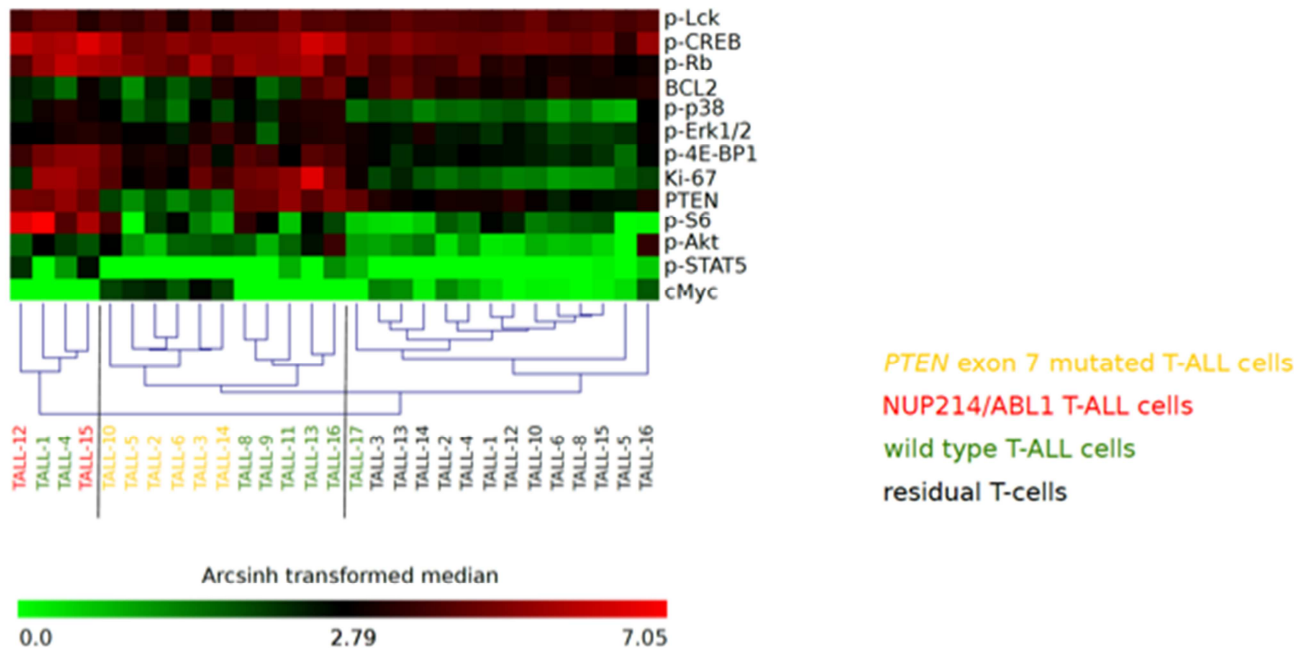


Figure S5: Levels of p-STAT5 in unstimulated T-ALL samples does not differ between IL-7 responder T-ALL and IL-7 nonresponder T-ALL samples

Median intensity evaluated by mass cytometry of p-STAT5 in unstimulated T-ALL cells obtained from bone marrow of IL-7 responder T-ALL patients (n=6, circles) and IL-7 nonresponder T-ALL patients (n=10, squares) are shown. The group of IL-7 nonresponder T-ALL patients includes the two patients with *NUP214/ABL1* gene fusion causing hyper-phosphorylation of p-STAT5.

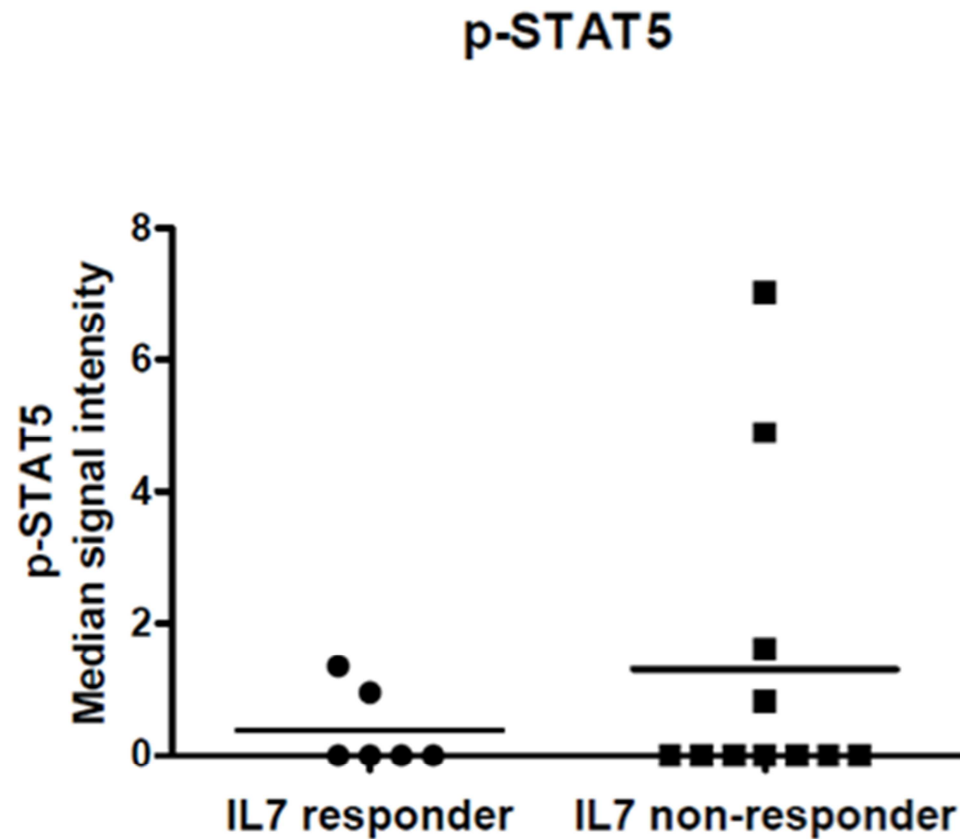


Figure S6: Two types of response to IL-7 were observed in T-ALL samples

IL-7 induced STAT5 phosphorylation (bottom) compared to their basal state (top) of T-ALL cells in one representative IL-7 responder, IL-7 nonresponder T-ALL sample (red histograms) and in residual T-cells (blue histograms)

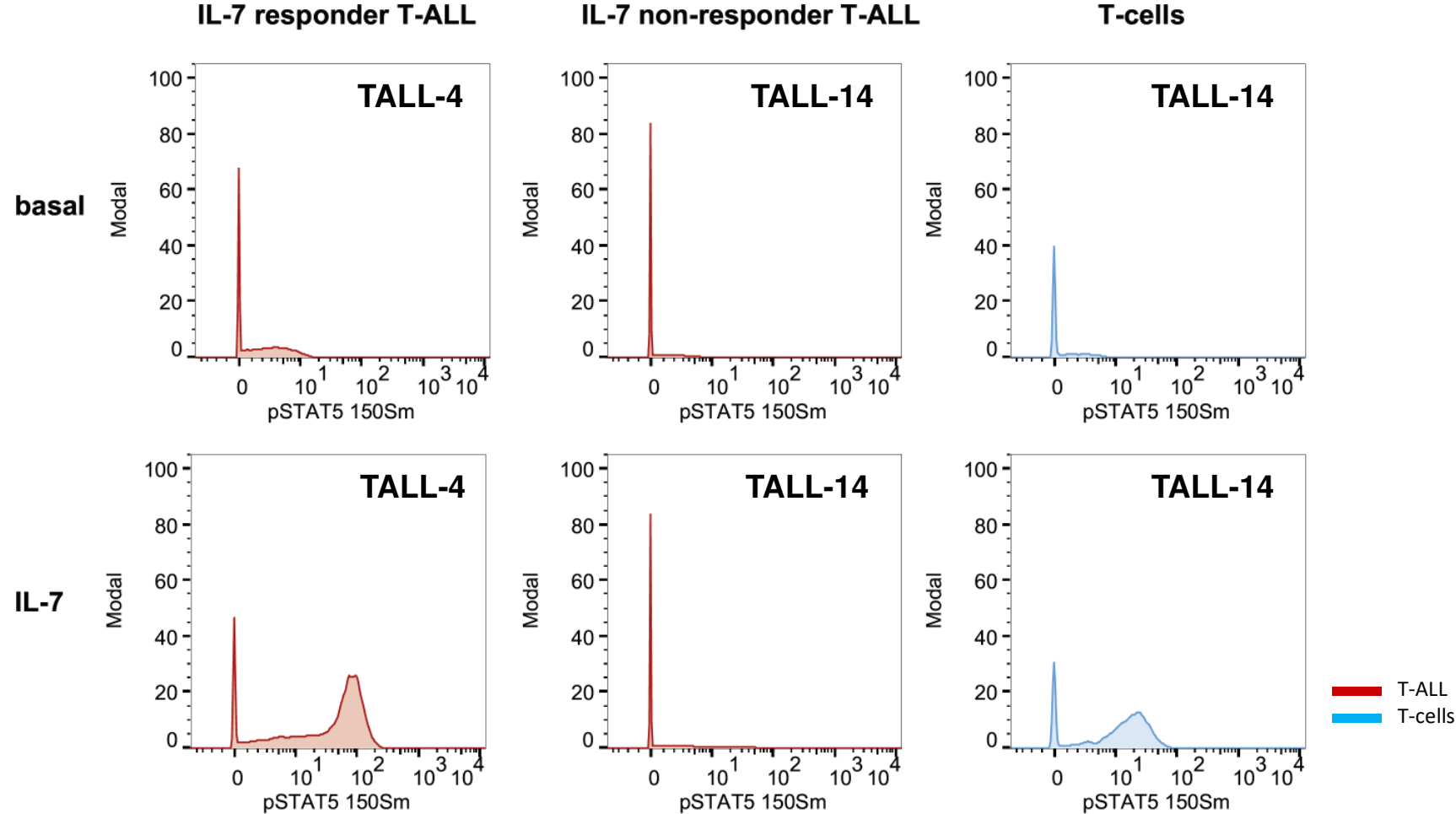


Figure S7: Ex vivo IL-7 stimulation of T-ALL cells induces STAT5 phosphorylation, no other node tested were affected

Median intensity evaluated by mass cytometry of p-4E-BP, p-STAT5, p-AKT, BCL-2, p-p38, p-S6, p-LCK, p-CREB, p-RB, Ki-67, p-ERK1/2, PTEN, MYC in gated T-ALL cells obtained from bone marrow of T-ALL patients (n=16) in unstimulated (circles) and ex vivo IL-7 stimulated (squares) are shown.

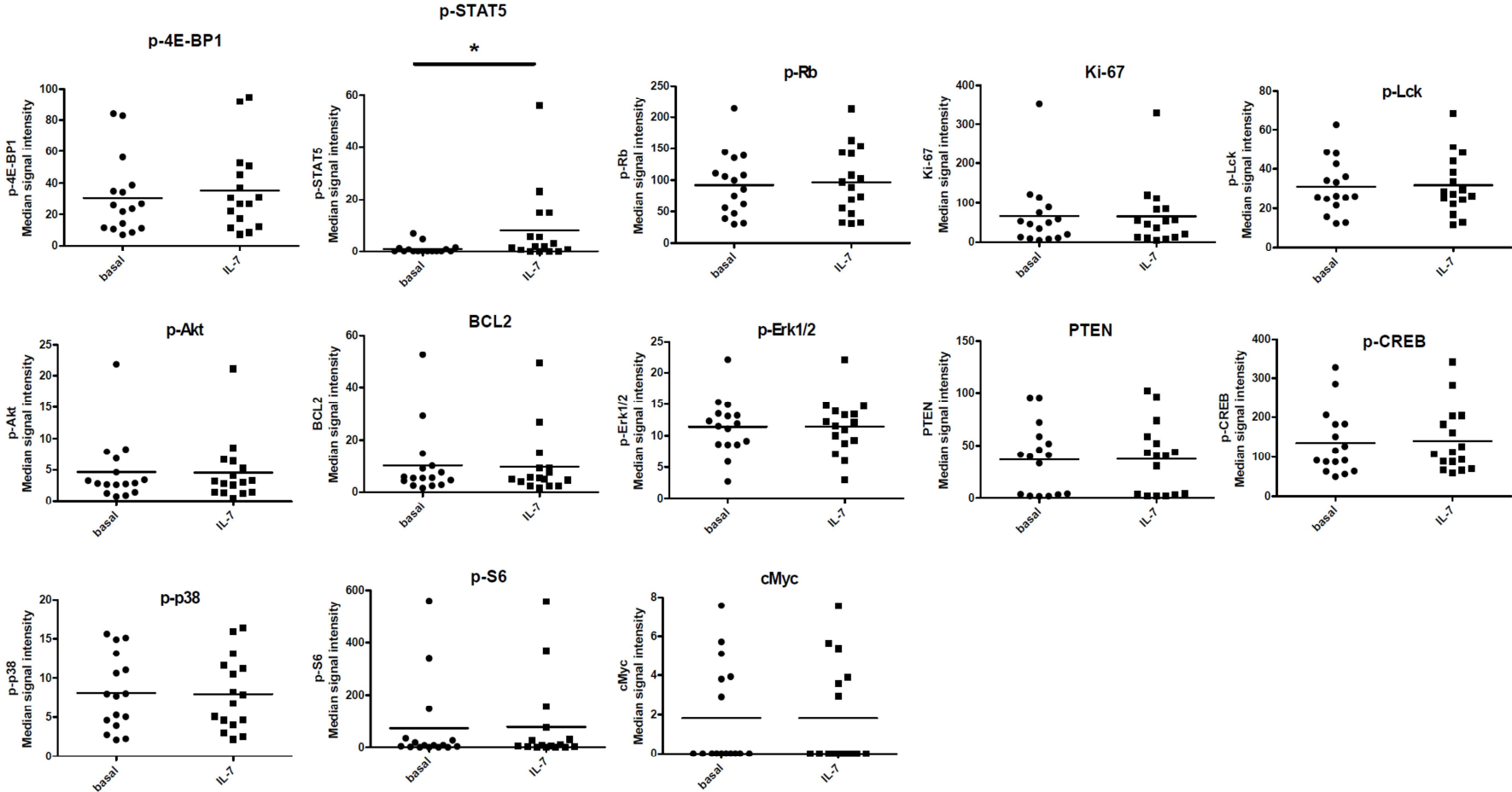


Figure S8: IL-7 induced STAT5 phosphorylation is not dependent on CD132 (common γ chain, subunit of IL-7R) expression

Correlation graph between percentage of surface CD132 (common γ chain, subunit of IL-7R) expression evaluated by flow cytometry and fold change of p-STAT5 after ex vivo IL-7 stimulation in T-ALL samples (red dots) and residual T-cells (blue dots) obtained from T-ALL patients at diagnosis.

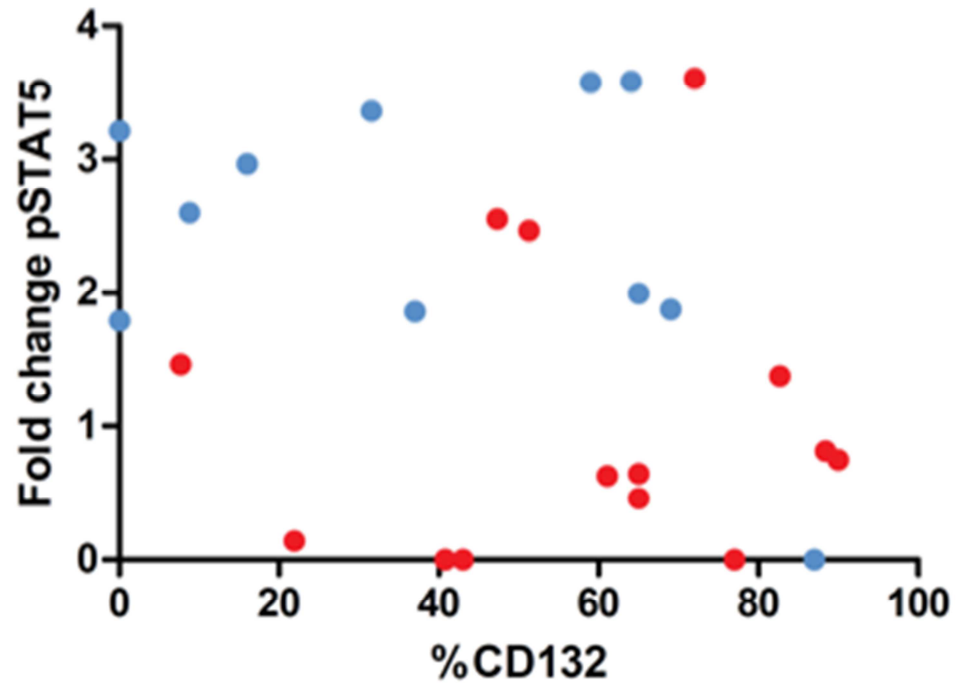


Figure S9: IL-7 responder T-ALL samples show higher levels of proliferation markers p-RB and Ki-67 compared to IL-7 nonresponder T-ALL samples

Median intensity evaluated by mass cytometry of p-4E-BP, p-STAT5, p-AKT, BCL-2, p-p38, p-S6, p-LCK, p-CREB, p-RB, Ki-67, p-ERK1/2, PTEN, MYC in unstimulated T-ALL cells obtained from bone marrow of IL-7 responder T-ALL samples (n=6, circles) and IL-7 nonresponder T-ALL samples (n=10, squares) are shown.

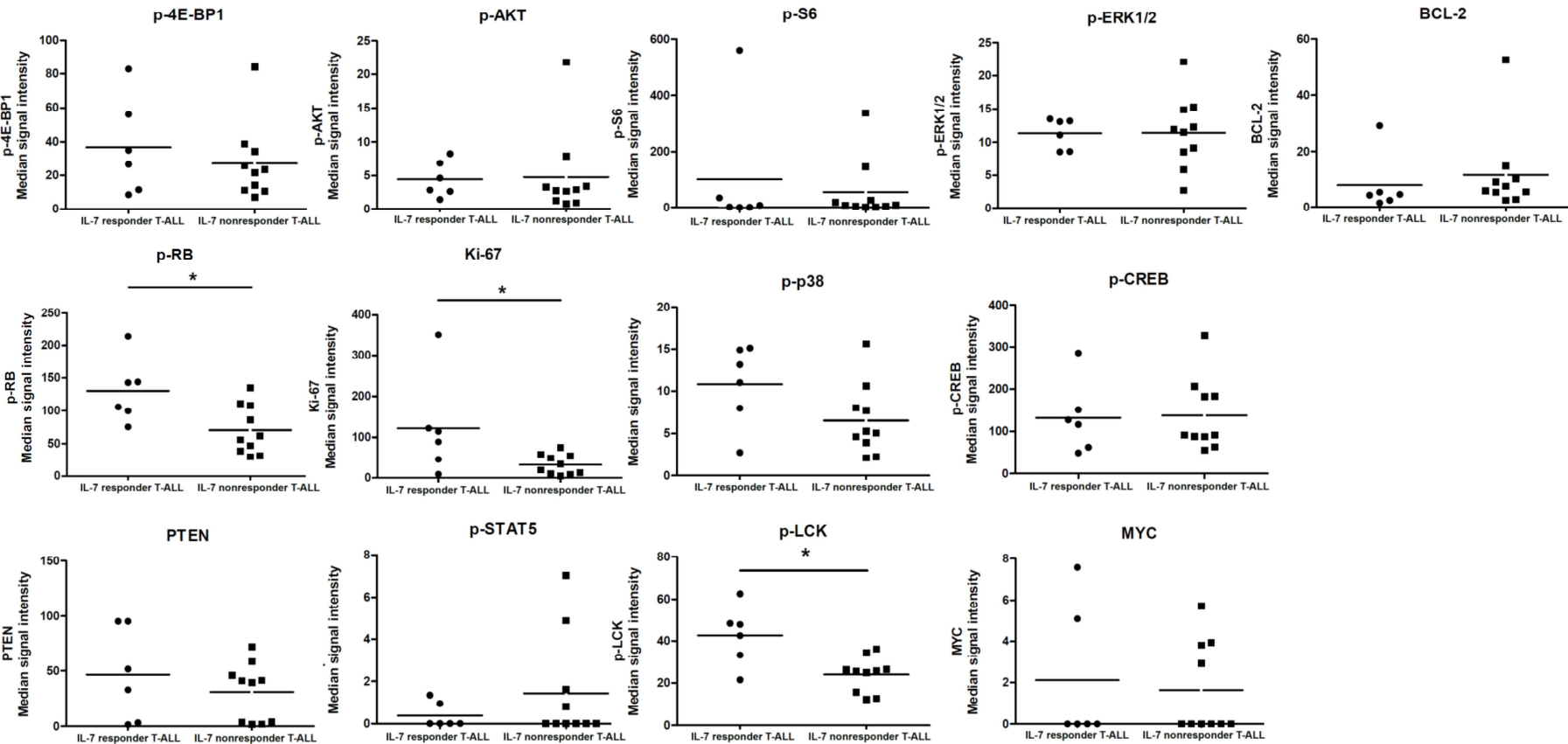


Figure S10: Ex-vivo response to IL-7 induces an increased cell viability and correlates with sensitivity to prednisolone

Absolute viable cell number in IL-7 responders (n=5) and IL-7 nonresponders (n=5) primary diagnostic T-ALL samples exposed for 48 hours to 50 ng/mL IL-7 (A), 50 ug/mL Methylprednisolone (PRED) alone or in combination with IL-7 (B-C) relative to untreated cells. Statistical significance was assessed using two-sample t-tests.

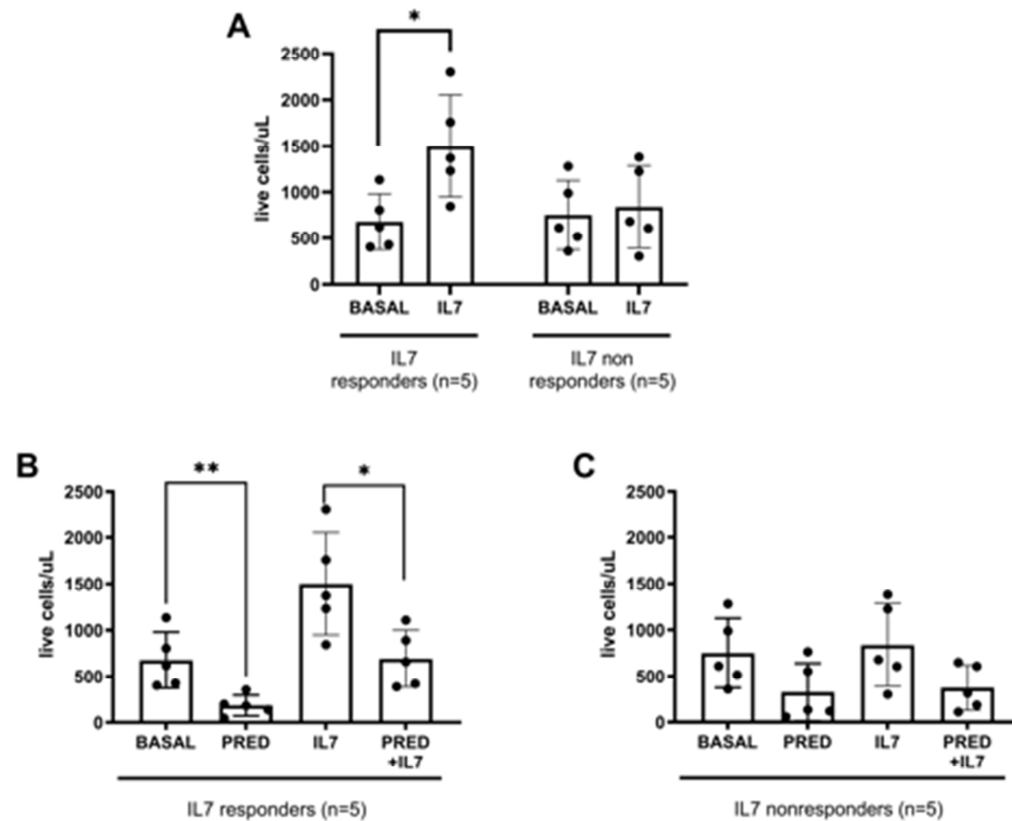


Figure S11: BEZ-235 responder T-ALL samples show higher level of inhibitory phosphorylation of LCK kinase compared to BEZ-235 nonresponder T-ALL samples

Median intensity evaluated by mass cytometry of p-4E-BP, p-STAT5, p-AKT, BCL-2, p-p38, p-S6, p-LCK, p-CREB, p-RB, Ki-67, p-ERK1/2, PTEN, MYC in unstimulated T-ALL cells obtained from bone marrow of BEZ-235 responder T-ALL samples (n=11, circles) and BEZ-235 nonresponder T-ALL samples (n=5, squares) are shown.

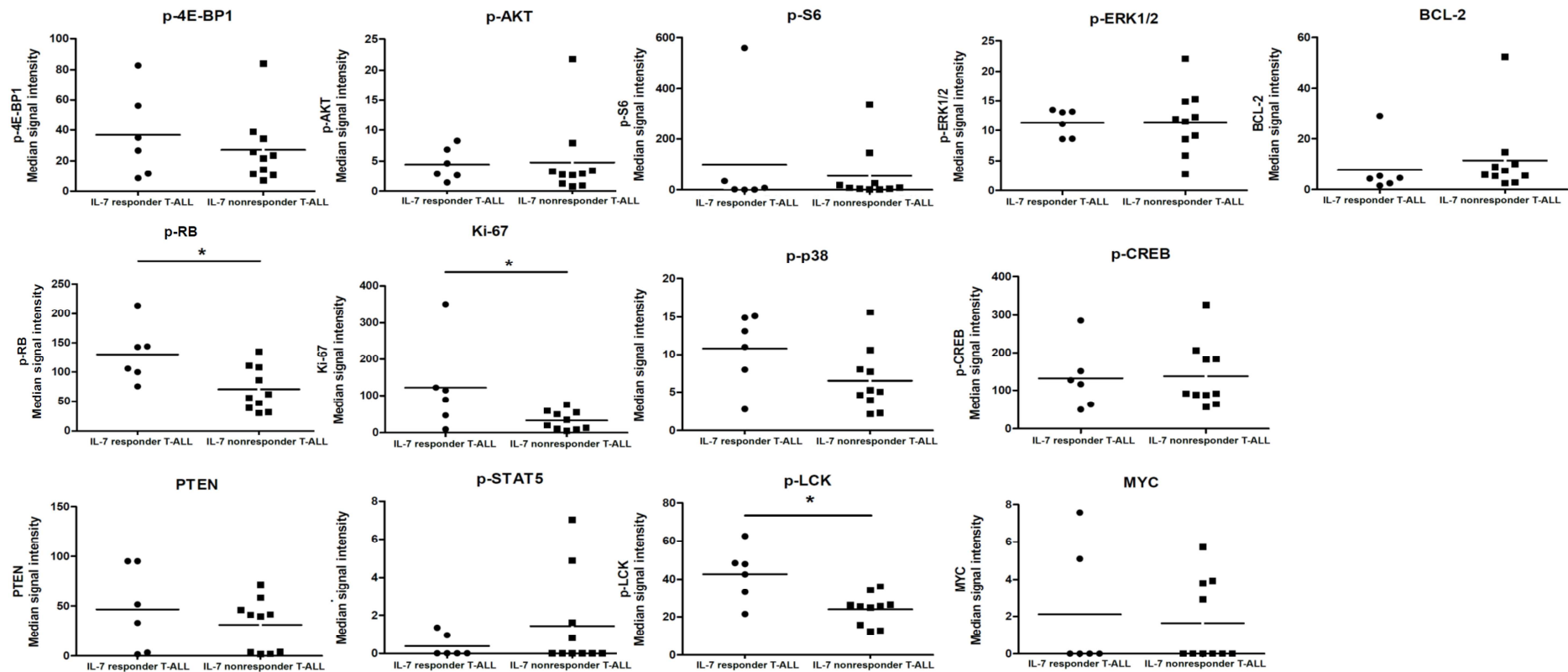


Figure S12: BEZ-235 signaling responsiveness does not correlate with drug responsiveness and the addition of BEZ-235 to the PRED treatment does not increase cell sensitivity to glucocorticoids

Absolute viable cell number of 8 primary diagnostic T-ALL samples (IL-7 responders n=4, IL-7 nonresponders n=4) exposed for 48 hours to 800nM BEZ-235, 50 ug/mL Methylprednisolon or both treatments relative to untreated cells. Statistical significance was assessed using two-sample t-tests.

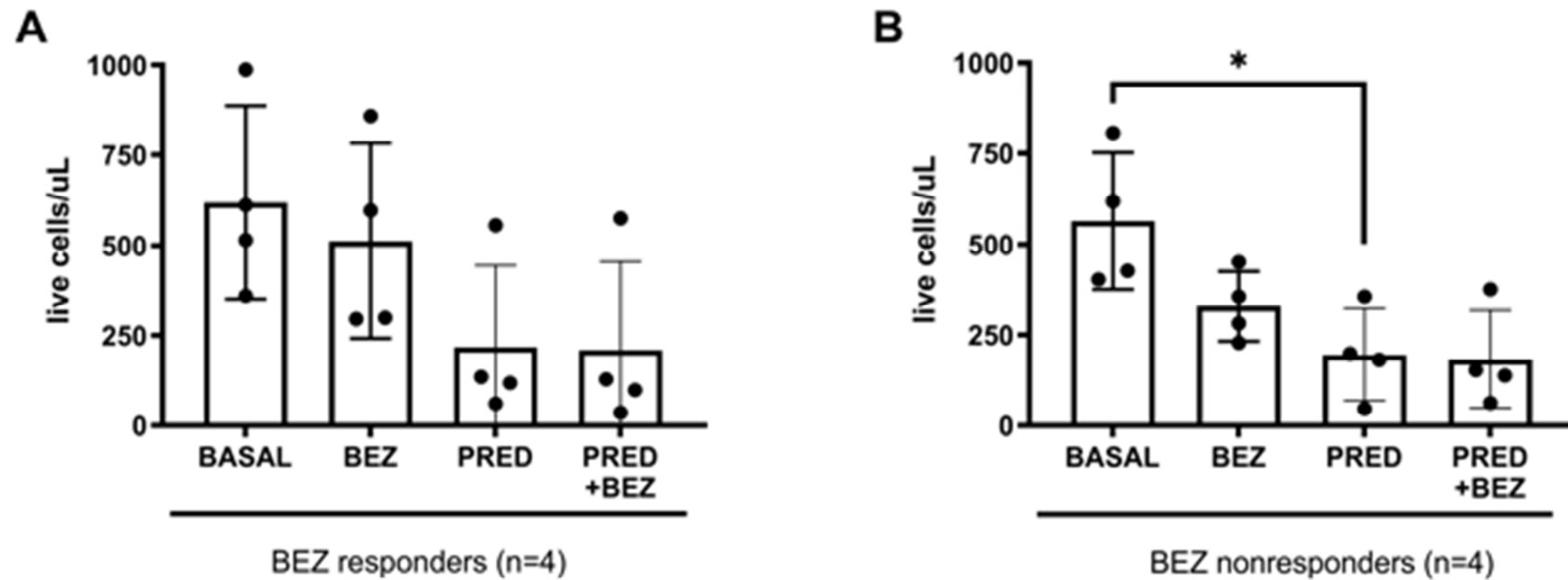


Figure S13: Vaevictis dimensionality reduction reveals the impact of expression/phosphorylation of intracellular regulators on phospho-signature patterns in paired diagnostic-relapse samples of pediatric T-ALL

Vaevictis dimensionality reduction was applied on T-ALL cells obtained from 5 pediatric T-ALL patients at diagnosis and relapse (top row). Gates were applied according to subsets based on dimred1 and dimred2 (Figure 6A). Signaling, proliferation and internal regulators (PTEN, MYC, BCL-2, p-4E-BP1, p-STAT5, p-AKT, p-p38, p-S6, p-LCK, p-CREB, p-RB, Ki-67, p-ERK1/2) were considered for the projection calculation. The heat corresponds with expression/phosphorylation of marker indicated above each set of projections, note the scale max differ for each sample.

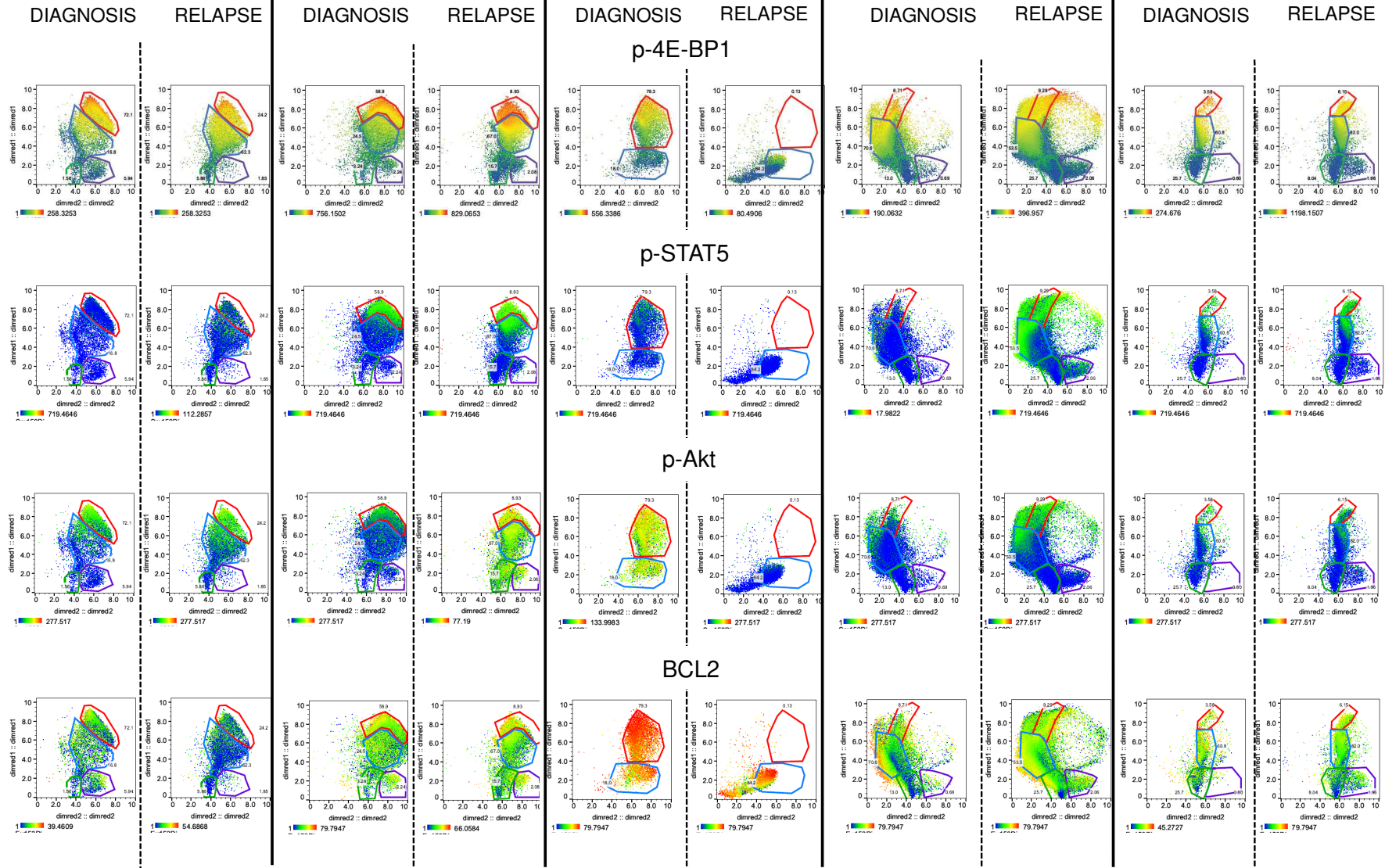
TALL-1

TALL-15

TALL-16

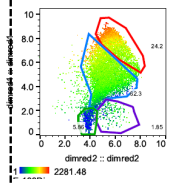
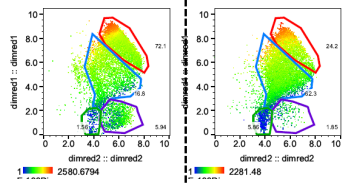
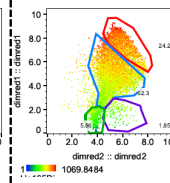
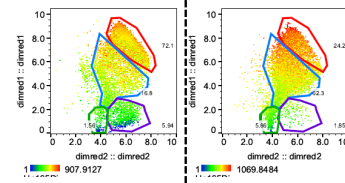
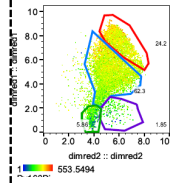
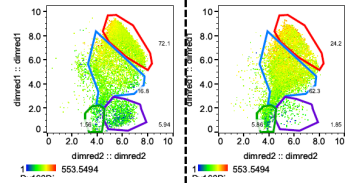
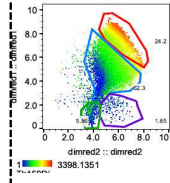
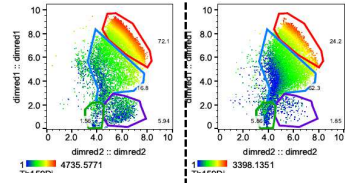
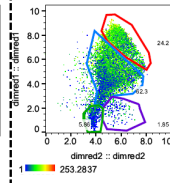
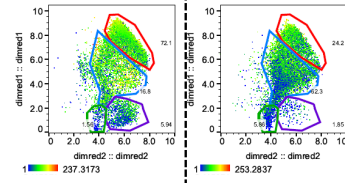
TALL-2

TALL-17



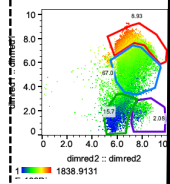
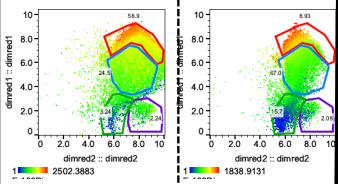
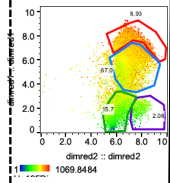
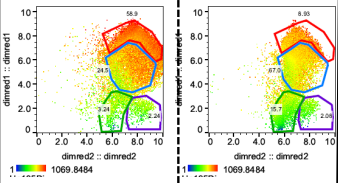
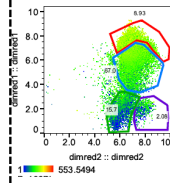
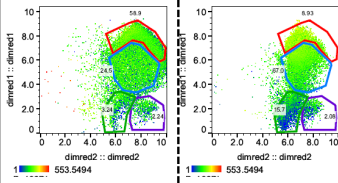
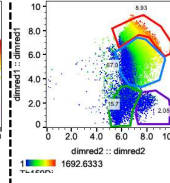
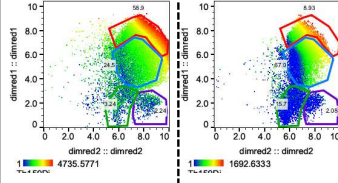
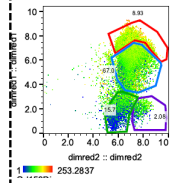
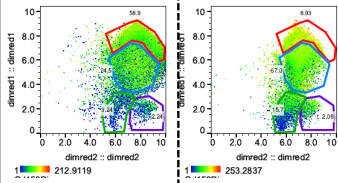
TALL-1

DIAGNOSIS RELAPSE



TALL-15

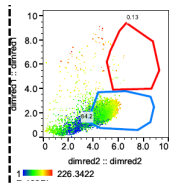
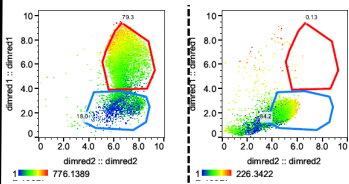
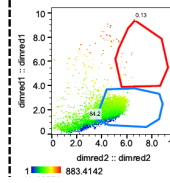
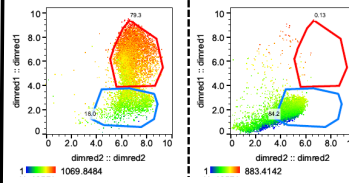
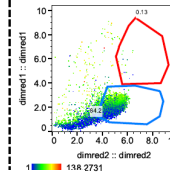
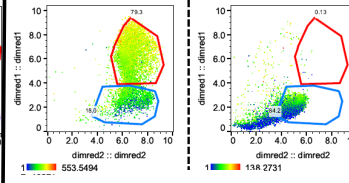
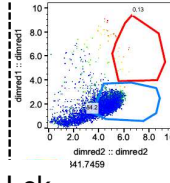
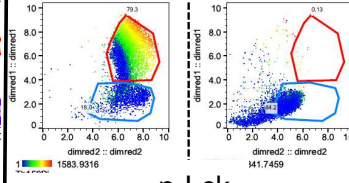
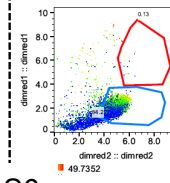
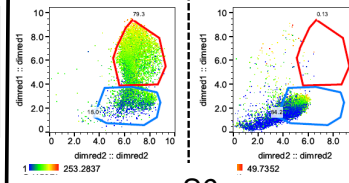
DIAGNOSIS RELAPSE



TALL-16

DIAGNOSIS RELAPSE

p-p38



p-S6

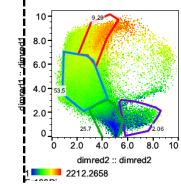
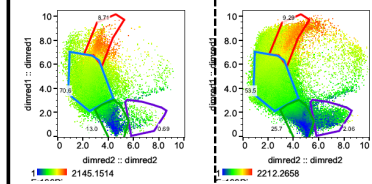
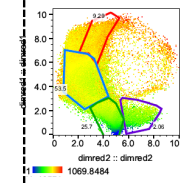
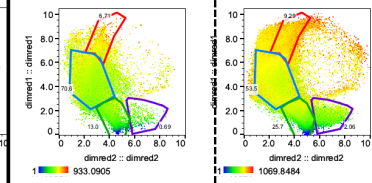
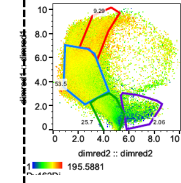
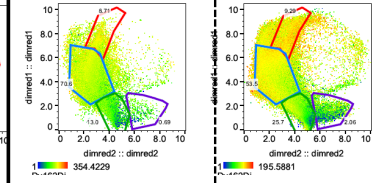
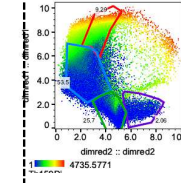
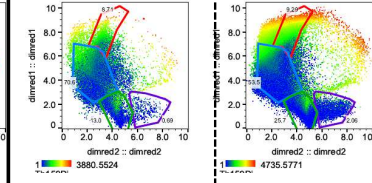
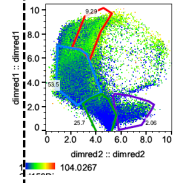
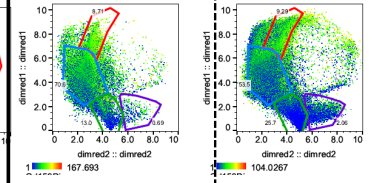
p-Lck

p-CREB

p-Rb

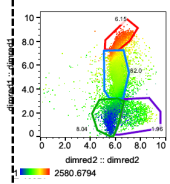
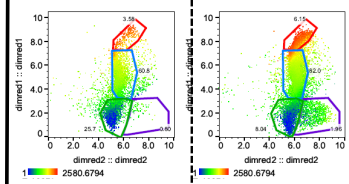
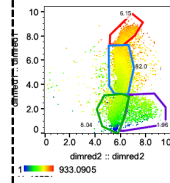
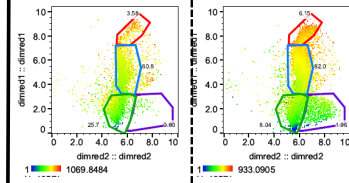
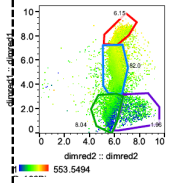
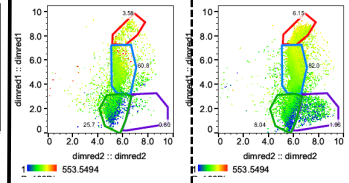
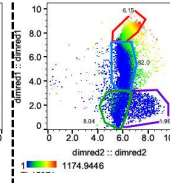
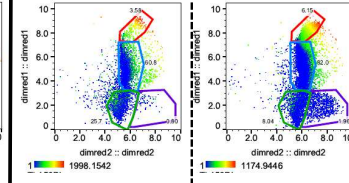
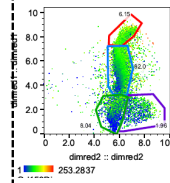
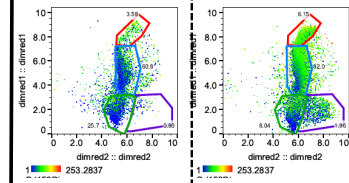
TALL-2

DIAGNOSIS RELAPSE



TALL-17

DIAGNOSIS RELAPSE



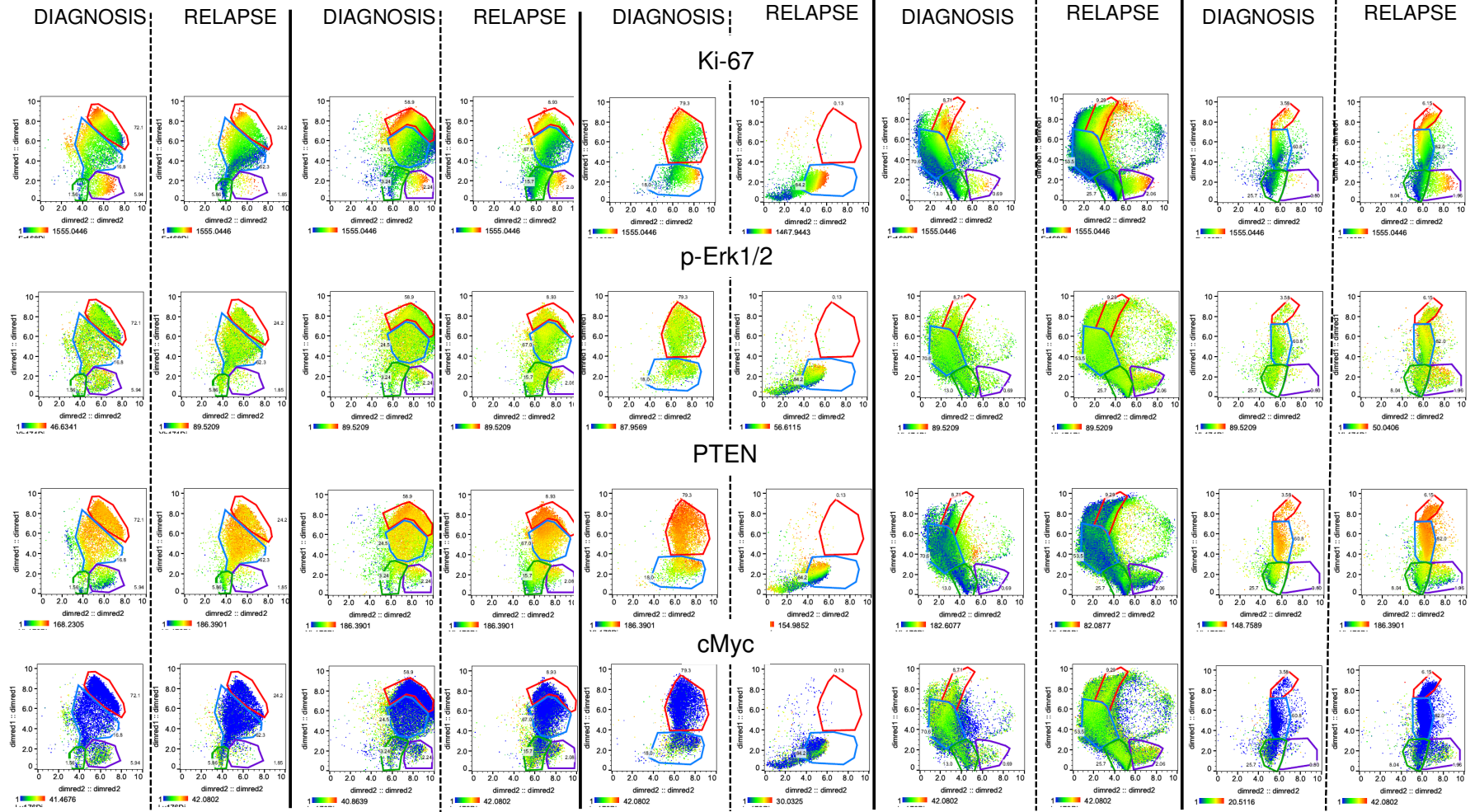
TALL-1

TALL-15

TALL-16

TALL-2

TALL-17



Supplementary References

1. Mei HE, Leipold MD, Schulz AR, Chester C, Maecker HT. Barcoding of live human PBMC for multiplexed mass cytometry. *J Immunol.* 2015;194(4):2022–2031.
2. Mei HE, Leipold MD, Maecker HT. Platinum-conjugated antibodies for application in mass cytometry. *Cytom Part A.* 2016;89(3):292–300.
3. Basso G, Veltroni M, Valsecchi MG, et al. Risk of Relapse of Childhood Acute Lymphoblastic Leukemia Is Predicted By Flow Cytometric Measurement of Residual Disease on Day 15 Bone Marrow. *J Clin Oncol.* 2009;27(31):5168–5174.